

20-80nm Channel Length InGaAs Gate-all-around Nanowire MOSFETs with EOT=1.2nm and Lowest SS=63mV/dec

J. J. Gu,¹⁾ X. W. Wang,²⁾ H. Wu,¹⁾ J. Shao,³⁾ A. T. Neal,¹⁾ M. J. Manfra,³⁾ R. G. Gordon,²⁾ and P. D. Ye¹⁾

¹⁾ School of Electrical and Computer Engineering and Birck Nanotechnology Center, Purdue University, West Lafayette, IN 47906, U.S.A.

²⁾ Department of Chemistry and Chemical Biology, Harvard University, Cambridge, MA 02138, U.S.A.

³⁾ Department of Physics, Purdue University, West Lafayette, IN, 47906, U.S.A.

Tel: 1-765-494-7611, Fax: 1-765-496-7443, Email: yep@purdue.edu, jiju@purdue.edu

Abstract

In this paper, 20nm - 80nm channel length (L_{ch}) InGaAs gate-all-around (GAA) nanowire MOSFETs with record high on-state and off-state performance have been demonstrated by equivalent oxide thickness (EOT) and nanowire width (W_{NW}) scaling down to 1.2nm and 20nm, respectively. SS and DIBL as low as 63mV/dec and 7mV/V have been demonstrated, indicating excellent interface quality and scalability. Highest $I_{ON} = 0.63\text{mA}/\mu\text{m}$ and $g_m = 1.74\text{mS}/\mu\text{m}$ have also been achieved at $V_{DD}=0.5\text{V}$, showing great promise of InGaAs GAA technology for 10nm and beyond high-speed low-power logic applications.

Introduction

Recently, a top-down technology for III-V GAA nanowire MOSFETs has been demonstrated [1-2]. However, the device metrics such as g_m , V_{DD} , SS, DIBL, and the L_{ch} scaling of the III-V GAA devices demonstrated in [1] are still greatly limited by the large EOT of the devices. In this paper, we experimentally demonstrate InGaAs GAA nanowire MOSFETs with an EOT down to 1.2nm by the successful integration of ternary oxide dielectric LaAlO₃ ($k \sim 16$) [3]. The reduction of EOT has allowed the demonstration of the first 20nm L_{ch} InGaAs MOSFETs with g_m as high as 1.74mS/ μm at $V_{ds}=0.5\text{V}$ and negligible short channel effects (SCE). A systematic scaling metrics study with L_{ch} between 20-80nm and nanowire size-dependent transport study with W_{NW} between 20-35nm has also been carried out for three different gate stacks, demonstrating near-ideal SS=63mV/dec and DIBL=7mV/V. It is shown that the integration of 4nm LaAlO₃ with ultra-thin 0.5nm Al₂O₃ interfacial layer allow reduction of EOT to 1.2nm with optimized interface trap density (D_{it}), offering excellent scalability, near-ballistic transport, and high g_m at low supply voltage.

Experiment

Fig. 1 shows a diagram of an InGaAs GAA nanowire MOSFET fabricated in this work. The starting material is a 30nm lightly p-doped InGaAs channel layer, an 80nm undoped InP sacrificial layer, and a 100nm undoped InAlAs etch stop layer on semi-insulating InP (100) substrate grown by molecular beam epitaxy (MBE). The InGaAs channel layer consists of 10nm In_{0.53}Ga_{0.47}As layer sandwiched by two 10nm In_{0.65}Ga_{0.35}As layers to boost the channel mobility and reduce the D_{it} . Key device dimensions are shown in Fig.

1 and the process flow is shown in Fig. 2. The three gate stacks studied are highlighted in Figs. 1-2. Samples A and B have a 0.5nm Al₂O₃/4nm LaAlO₃ stack (EOT = 1.2nm), where Al₂O₃ was grown before LaAlO₃ for sample A and vice versa for sample B in order to study the effect of ultra-thin Al₂O₃ passivation layer on the LaAlO₃/InGaAs interface quality. Sample C has 3.5nm Al₂O₃ gate (EOT = 1.7nm). The fabrication process is similar to that demonstrated in [1]. The additional InAlAs bottom layer provides better control of the selective wet etching in the nanowire release process and cuts off parasitic leakage through the substrate. The Al₂O₃/LaAlO₃/WN high-k/metal gate stacks were all deposited by atomic layer deposition (ALD) in a tubular reactor without air break between layers. A short-time buffered oxide etch and 10% (NH₄)₂S passivation were performed before transferring the samples to the ALD reactor. The Al₂O₃ and LaAlO₃ were grown at 300 °C and the WN was grown at 385°C. Lanthanum tris(*N,N'*-diisopropylformamidinate), trimethylaluminum, and H₂O were used as the precursors for LaAlO₃ deposition, while bis(*tert*-butylimido)bis(dimethylamido)tungsten(VI) vapor and ammonia gas were used as the WN precursors. The sheet resistance of the ALD WN film was measured by a four-point probe station, and the resistivity was 2.2 mΩ·cm for a 40 nm WN film. The excellent conformity and uniformity of the ALD process is critical for realizing the GAA structure with ultra-small EOT. The L_{ch} is varied from 80nm down to 20nm, W_{NW} is varied from 35nm down to 20nm with a fixed nanowire height (H_{NW}) of 30nm defined by the MBE thickness. The nanowire length (L_{NW}) is fixed at 200nm. Four parallel wires are integrated in each device. The nanowires are aligned along [100] direction as required by the anisotropic release process, which also defines the transport direction of the GAA devices. Fig. 3 shows the top-view SEM images of the 20nm PMMA mask defining the smallest L_{ch} and a finished GAA device. Note that due to the dopant diffusion, the actual L_{ch} is smaller than the defined L_{ch} . All patterns were defined by a Vistec VB6 UHR electron beam lithography system and dry etching was performed with a Panasonic E620 high density plasma etcher. The MOSFET electrical characterization was performed using a Keithley 4200 at room temperature.

Results and Discussion

Fig. 4-6 show the well-behaved output characteristics, transfer characteristics, and g_m - V_{gs} of a GAA FET (sample A) with $L_{ch} = W_{NW} = 20\text{nm}$. The current is normalized by the

total perimeter of the nanowires, i.e. $W_G = 2 \times (W_{NW} + H_{NW})$ \times (Wire Number). The 20nm L_{ch} device shows negligible channel length modulation, $I_{ON} = 850\mu A/\mu m$ at $V_{DD} = 0.8V$, $g_m = 1.65mS/\mu m$ at $V_{ds} = 0.5V$, SS = 75mV/dec and DIBL = 40mV/V. The device operates in enhancement-mode with $V_T = 0.14V$ extracted by linear extrapolation at $V_{ds} = 0.05V$. Fig. 7 shows the SS scaling metrics for sample A with $W_{NW} = 20nm$. Error bars show the standard deviation of the measurement over 25 devices at each data point. Consistent sub-100mV/dec SS has been obtained for the devices at $V_{ds}=0.5V$ for all L_{ch} . Figs. 8 - 9 show the SS and DIBL scaling metrics with different W_{NW} . No evident W_{NW} dependence is observed, indicating the current EOT and GAA structure yield a very small geometric screening length (λ) compared to L_{ch} . The mean SS and DIBL remain unchanged at ~75mV/dec and ~25mV/V with L_{ch} down to 50nm, showing the immunity of these devices to SCE.

Fig. 10 shows the transfer characteristics of one of the three best devices with SS of 63mV/dec at $V_{ds}=0.05V$, indicating excellent gate control and low D_{it} . Seventeen devices show SS below 70mV/dec. The lowest DIBL achieved is 7mV/V (not shown). Figs. 11 - 12 show that g_m and I_{ON} remain constant at small L_{ch} indicating near-ballistic transport. Fig. 13 shows the D_{it} box plot and histogram of sample A. The midgap D_{it} is extracted from the SS at $V_{ds} = 0.05V$ for $L_{ch} = 50 - 80nm$ since these devices are immune to SCE. A mean D_{it} of $\sim 4 \times 10^{12} eV^{-1}cm^{-2}$ is obtained with the lowest value of $9 \times 10^{11} eV^{-1}cm^{-2}$ corresponding to the 63mV/dec device. Fig. 14 shows the increasing g_m and I_{on} with decreasing W_{NW} , due to the quantum confinement and volume inversion effect [2]. Simulation of inversion charge distribution inside the InGaAs nanowires in Fig. 15 (a) confirms volume inversion at all W_{NW} . Fig. 15 (b) shows the inversion layer distribution along $y = 15nm$ for different W_{NW} . It is projected that the optimum W_{NW} occurs at around 10nm where a plateau across the entire nanowire would form. Further reduction of nanowire size is therefore required to study the ultimate performance limit of InGaAs GAA devices.

Figs. 16 - 17 show the transfer characteristics and g_m-V_{gs} for 20nm L_{ch} InGaAs GAA MOSFETs with EOT = 1.7nm (sample C). Increasing EOT has led to increased SCE, evident from the larger SS and DIBL. However, higher $g_m = 1.8mS/\mu m$ at $V_{ds} = 0.5V$ and $2.1mS/\mu m$ at $V_{ds} = 1V$ is obtained on sample C, indicating enhanced mobility with relaxed EOT. A negative $V_T = -0.138V$ is also obtained from the same device. Fig. 18 shows the relatively low gate leakage current density for EOT=1.2 and 1.7nm even with the advanced 3D structure. Figs. 19 - 21 show the SS, DIBL, and V_T scaling metrics for sample A, B, and C with L_{ch} ranging from 20 to 80nm. Sample C shows the largest SS and DIBL due to the larger EOT of 1.7nm. Sample B shows worse SS and DIBL compared to sample A with the same EOT = 1.2nm due to the larger D_{it} [3]. This indicates that insertion of ultra-thin Al_2O_3 interfacial layer can effectively improve

$LaAlO_3/InGaAs$ interface quality. Decreasing EOT also results in better V_T roll-off properties and is favorable for an enhancement-mode operation. It is also noted that the variation of sample A is also the least among all three gate stacks. This indicates that the EOT scaling with effective interface passivation has led to not only scalability improvements but also a variability breakthrough. Detailed analysis of the variability and reliability of InGaAs nanowire devices is on-going. Fig. 22 benchmarks SS and DIBL in this work with InGaAs non-planar FETs fabricated in our group. The GAA structure with thin EOT has shown significant improvement in the control of SCE, due to the better gate control. Table 1 compares the device dimensions and performance in this work with the representative non-planar and thin body planar InGaAs MOSFETs in the literature [4-8]. The successful demonstration of the smallest L_{ch} , W_{NW} , SS, DIBL and highest g_m has been achieved in this work.

Conclusion

We have demonstrated the shortest $L_{ch}=20nm$ InGaAs GAA nanowire MOSFETs with ALD $Al_2O_3/LaAlO_3$ gate stack. Lowest SS of 63mV/dec and DIBL of 7mV/V have been achieved. Benefiting from both the ultimate scalability of GAA structure and excellent transport property of III-V channel, InGaAs GAA technology is a strong candidate for future high-speed low-power logic applications.

Acknowledgement

The authors would like to thank Y. Q. Wu, X. L. Li, M. S. Lundstrom, D. A. Antoniadis, and J. A. del Alamo for the valuable discussions. This work is supported by the SRC FCRP MSD Center, NSF and AFOSR.

References

- [1] J. J. Gu *et. al.*, "First Experimental Demonstration of Gate-all-around III-V MOSFETs by Top-down Approach", *IEDM Tech. Dig.* 769 (2011).
- [2] J. J. Gu *et. al.*, "Size-dependent-transport Study of $In_{0.53}Ga_{0.47}As$ Gate-all-around Nanowire MOSFETs: Impact of Quantum Confinement and Volume Inversion", *IEEE Electron Device Lett.* 33, 967, (2012).
- [3] J. Huang *et. al.*, "InGaAs MOSFET performance and reliability improvement by simultaneous reduction of oxide and interface charge in ALD (La) AlO_x/ZrO_2 gate stack", *IEDM Tech. Dig.* 335 (2009).
- [4] M. Radosavljevic *et. al.*, "Electrostatics Improvement in 3-D Tri-gate Over Ultra-Thin Body Planar InGaAs Quantum Well Field Effect Transistors with High-K Gate Dielectric and Scaled Gate-to-Drain/Gate-to-Source Separation", *IEDM Tech. Dig.* 765 (2011).
- [5] K. Tomioka *et. al.*, "Vertical $In_{0.7}Ga_{0.3}As$ Nanowire Surrounding-Gate Transistors with High-k Gate Dielectric on Si Substrate", *IEDM Tech. Dig.* 773 (2011).
- [6] A. W. Dey *et. al.*, "High-Performance InAs Nanowire MOSFETs", *IEEE Electron Device Lett.*, 33, 791 (2012).
- [7] H.-C. Chin *et. al.*, "III-V Multiple-Gate Field-Effect Transistors With High-Mobility $In_{0.7}Ga_{0.3}As$ Channel and Epi-Controlled Retrograde-Doped Fin", *IEEE Electron Device Lett.* 32, 146 (2011).
- [8] S. Kim *et. al.*, "Sub-60 nm Deeply-Scaled Channel Length Extremely-thin Body $In_xGa_{1-x}As$ -On-Insulator MOSFETs on Si with Ni-InGaAs Metal S/D and MOS Interface Buffer Engineering", *VLSI Tech. Dig.* 177 (2012).

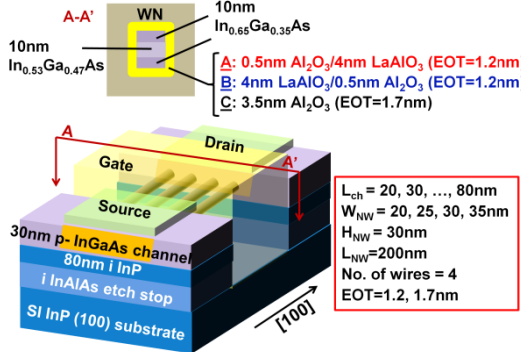


Fig. 1 Device structure, dimension and key parameters of InGaAs GAA MOSFETs.

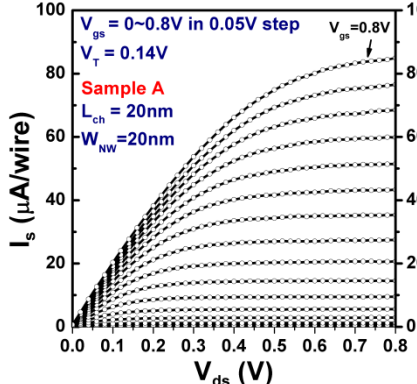


Fig. 4 Output characteristics of a 20nm L_{ch} InGaAs GAA MOSFET with $\text{Al}_2\text{O}_3/\text{LaAlO}_3$ gate dielectric (Sample A, EOT=1.2nm) and $W_{NW}=20\text{nm}$. I_s is used due to relatively large junction leakage current in I_d .



Fig. 2 Fabrication process flow and device splits of InGaAs GAA MOSFETs.

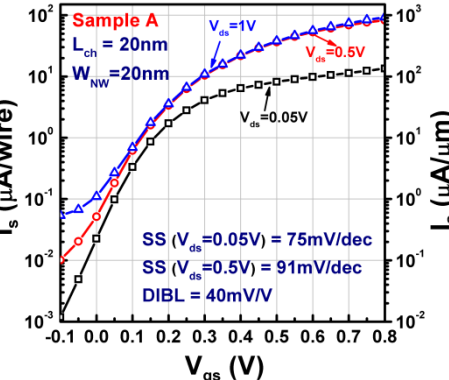


Fig. 5 Transfer characteristics of the same device shown in Fig. 4. $W_G=100\text{nm}$ for $W_{NW}=20\text{nm}$ normalized to perimeter.

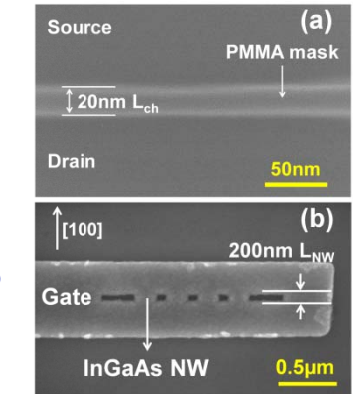


Fig. 3 SEM images of (a) PMMA mask defining 20nm L_{ch} (b) an InGaAs GAA FET with 4 wires.

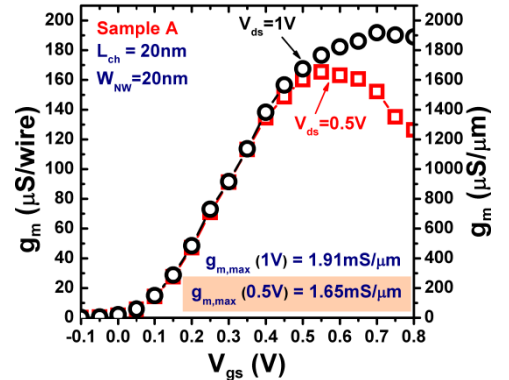


Fig. 6 Transconductance of the same device shown in Fig. 4.

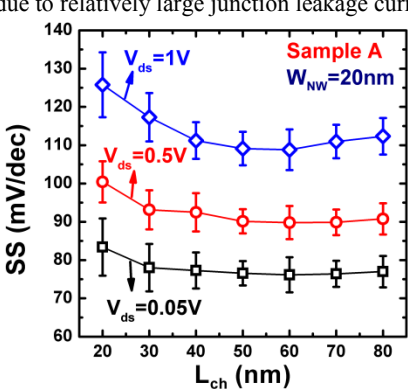


Fig. 7 SS scaling metrics for InGaAs GAA MOSFETs (Sample A, $W_{NW}=20\text{nm}$). Error bars show standard deviation of the measurements over 25 devices.

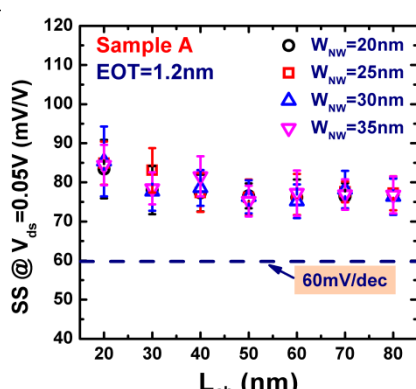


Fig. 8 SS ($V_{ds}=0.05\text{V}$) scaling metrics for sample A with W_{NW} from 20 to 35 nm.

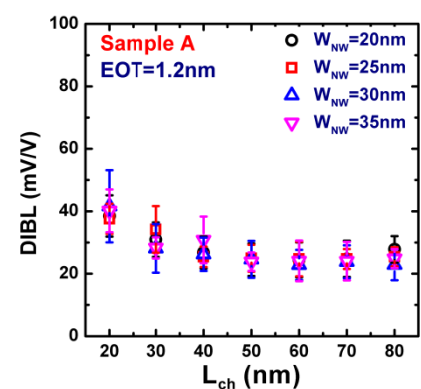


Fig. 9 DIBL scaling metrics for sample A with W_{NW} from 20 to 35 nm.

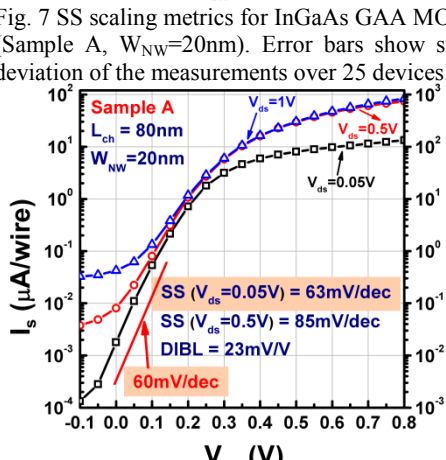


Fig. 10 Transfer characteristics of $L_{ch}=80\text{nm}$ InGaAs GAA MOSFET (Sample A, $W_{NW}=20\text{nm}$) with SS=63mV/dec at $V_{ds}=0.05\text{V}$. Three measured devices show SS=63mV/dec.

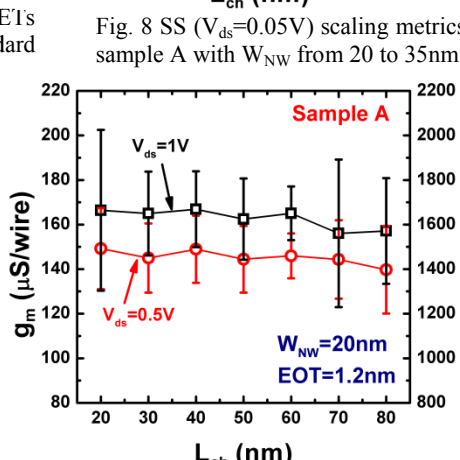


Fig. 11 g_m scaling metrics for sample A (EOT = 1.2nm, $W_{NW}=20\text{nm}$) at $V_{ds}=0.5\text{V}$ and 1V.

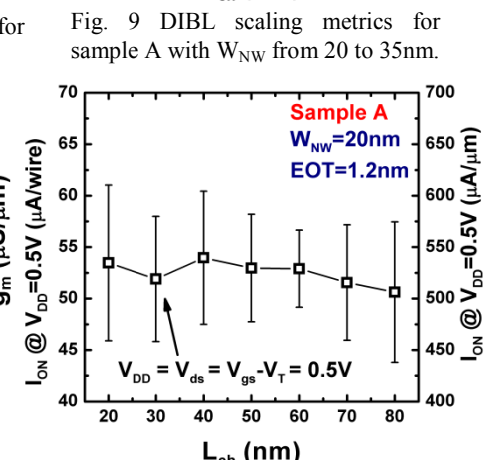
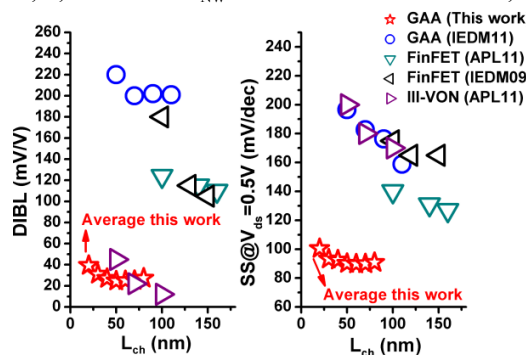
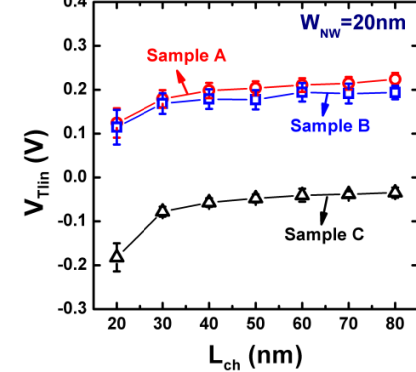
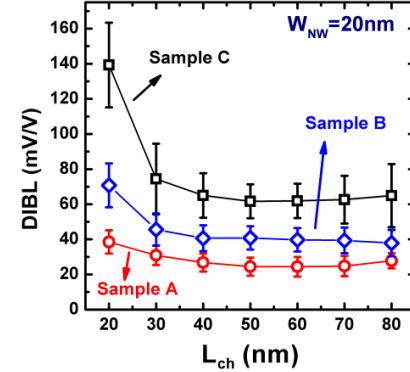
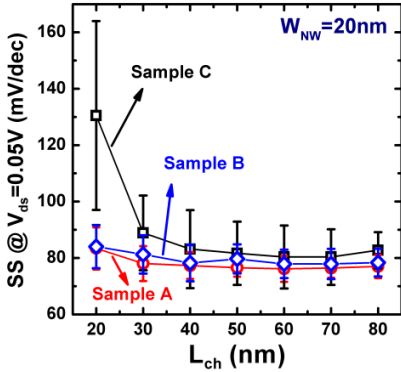
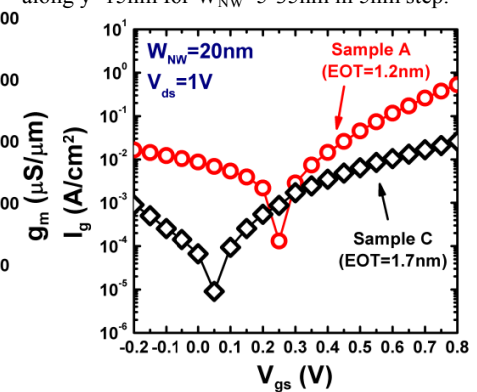
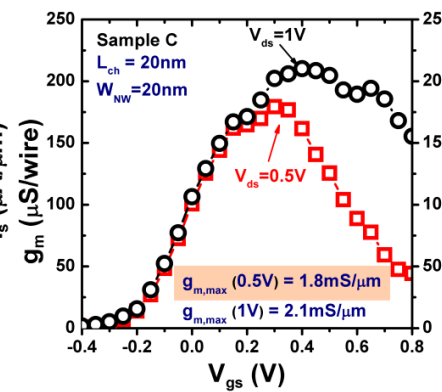
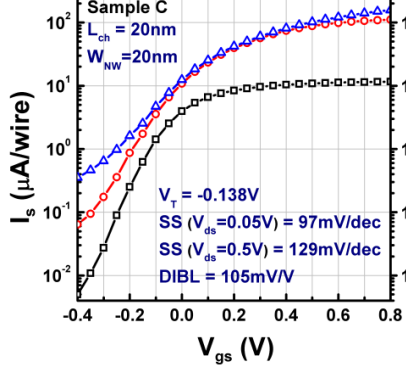
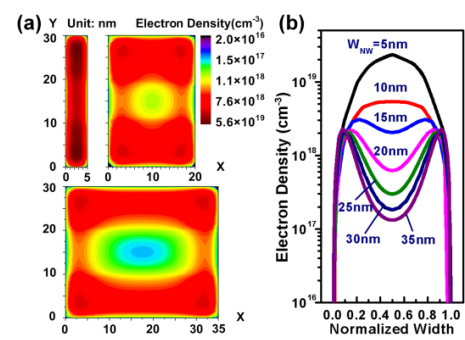
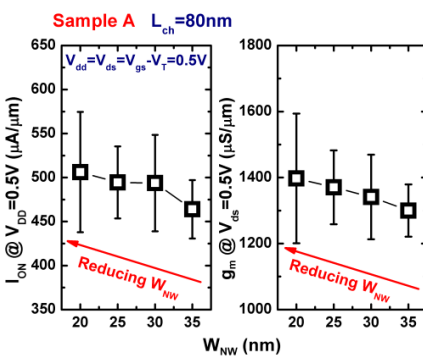
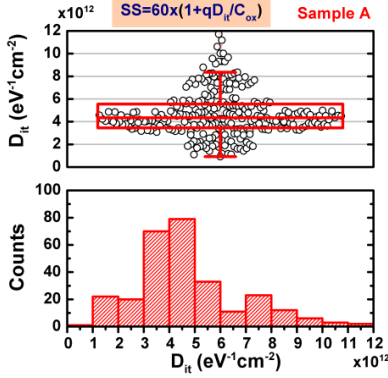


Fig. 12 I_{ON} scaling metrics for sample A (EOT = 1.2nm, $W_{NW}=20\text{nm}$) at $V_{ds}=V_{gs}-V_T=0.5\text{V}$.



	This work**	Ref. [1]	Ref. [4]	Ref. [5]	Ref. [6]	Ref. [7]	Ref. [8]
$In_xGa_{1-x}As$ (x)	0.65	0.53	0.7	0.7	1	0.7	1
Structure	GAA	GAA	Tri-gate	GAA	GAA	FinFET	ETB
Fabrication	Top-down	Top-down	Top-down	Bottom-up	Bottom-up	Top-down	Top-down
$L_{ch,min}$ (nm)	20	50	60	200	100	130	55
$W_{NW}(Fin)_min$ (nm)	20	30	30	90	15	220	-
EOT (nm)	1.2	4.5	1.2	1.8*	1.1*	4.5*	3.5
SS [$V_{dd}=0.5\text{V}$] (mV/dec)	88	245	94*	98	140	-	-
SS [$V_{dd}=0.5\text{V}$] (mV/dec)	63	145	66	90*	-	230*	105
DIBL (mV/V)	7	210	60*	170*	60	135	84
$g_{m,max}$ (mS/ μm) [$V_{ds}=0.5\text{V}$]	1.74	0.45	-	1.23	-	-	-

*Extracted/estimated from literature

**Reported values are best from all measured devices